ASEG-PESA 2015
Geophysics and Geology together for Discovery
24th International Geophysical Conference and Exhibition
15–18 February 2015 Perth, Western Australia

Operations Summary During Riserless Drilling to >7700 mbsl in the Japan Trench for IODP Expedition 343 & 343T JFAST and Discussion of the Relationship Between Drilling Parameters and Rock Damage.

Virginia Toy
Department of Geology
University of Otago
PO Box 56 Dunedin 9023
NEW ZEALAND
virginia.toy@otago.ac.nz

Sean Toczko
Nobu Eguchi
Lena Maeda
Ikuo Sawada
Tomokazu Saruhashi
CDEX, JAMSTEC
Showa-machi 3173-25, Kanazawa-ku
Yokohama 236-0001,
JAPAN
stoczko@jamstec.go.jp
neguchi@jamstec.go.jp
lmaeda@jamstec.go.jp
isawada@jamstec.go.jp
tsaruhashi@jamstec.go.jp

Fred Chester
Dept. Geology & Geophysics
Texas A&M University
College Station, TX 77843
USA
chesterf@tamu.edu

Jim Mori
Disaster Prevention Res. Inst.
Kyoto University
Gokasho, Uji, Kyoto 611-0011
JAPAN
mori@eqh.dpri.kyoto-u.ac.jp

SUMMARY

During IODP Expedition 343: The Japan Trench Fast Drilling Project (JFAST), five boreholes were drilled from the D/V *Chikyu* in >6800 m water depth. Three of these crossed the main fault target. A logging-while-drilling (LWD) hole that penetrated to 850.5 meters below seafloor (mbsf) (total depth [TD] = 7740 meters below sea level [mbsl]) was documented using a suite of LWD tools. From an adjacent partially cored hole drilled to 844.5 mbsf (TD = 7734 mbsl) 21 cores were acquired that spanned the two main fault targets. During the follow-up expedition 343T a third borehole was drilled to 854.8 mbsf (TD = 7752.3 mbsl) and a simple temperature observatory was deployed in the wellhead. The drilling operation, which lasted 88 days, was very technically challenging. Notably, the drill string had to be withdrawn a number of times due to high seas, and technical issues.

In certain intervals, rather than core we recovered loose, subrounded fine gravel clasts of the two major lithologies penetrated to those depths (silt and mudstone). Particle shape and size of these clasts was analysed. Results demonstrate (1) particle shape variations apparent visually are not easily quantified, (2) there are distinct variations in particle size distributions. We discuss whether these relate to variations in drilling parameters.

Key words: Ultra-deep water drilling, image analysis, rock mechanics, seismogenesis.

INTRODUCTION

Numerous challenges are associated with drilling in ultra-deep water as done by the International Ocean Discovery Program (IODP) vessel D/V *Chikyu*. This ship is capable of riser drilling in <2500 m of water, and non-riser drilling to much greater depths as was successfully carried out during Expedition 343: The Japan Trench Fast Drilling Project (JFAST). Notable challenges in ultra-deep water drilling that were overcome, included (i) setting and re-entering wellheads guided by an underwater television system, and (ii) core retrieval through >7000 m of drill string.

The recovered core was incomplete (43% recovery), probably due to 'jamming' in the barrel. In some intervals only fine gravel clasts were recovered. How can we determine if these were generated in weak formation by the drilling process, or by degeneration of the material during recovery of the partly empty core barrel? We have compared variations in drilling parameters (e.g. rate of penetration) with variations in particle size distribution of the recovered material, on the assumption that any correlation will implicate the former mechanism is correct, and discuss these results herein.

In general, particle size and shape *may* be uniquely correlated to the mechanical work expended in their generation (e.g. Chester et al., 1995; Stünitz et al., 2012), and examination of material generated by mechanical processes like drilling may reveal these relationships. However, we first need to establish that particle parameters can be correctly measured by automated techniques. In the recovered samples a shape difference between grey and brown clasts (different sedimentary protoliths) is apparent to the naked eye. We discuss whether these differences can also be resolved using systematic measurements from image analysis and combinations of these measurements into 'shape descriptors'.

CHALLENGES OF DEEP OCEAN DRILLING

Underwater television (UWTV)

The OCC Corporation UWTV system (maximum operational water depth = 7000 m) is equipped with 2 Kongsberg Simrad underwater low-light cameras, a Kongsberg Mesotech underwater sonar system, and two DeepSea underwater lamps. The entire system is powered through an armored umbilical cable containing 4 optical fibers and 4 copper conductors.

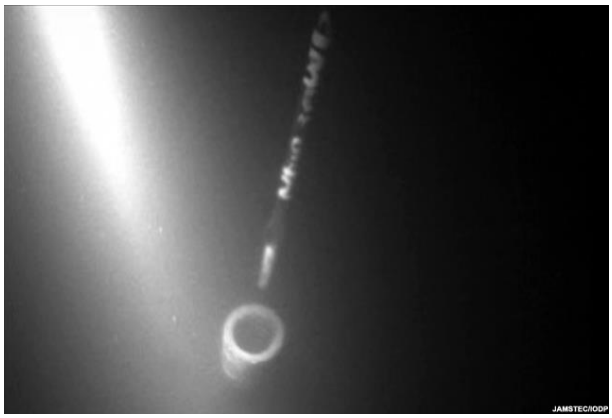

Figure 1. Example UWTV image of wellhead and drill string.

Rate of progress

During high seas (>5 m swells) the drill string had to be withdrawn. Re-entry of the borehole required visual alignment of the drill bit with the wellhead based on the UWTV image (Figure 1) in conjunction with the ship's dynamic positioning system. Re-entry and thus recommencement of drilling after storms was regularly delayed by malfunction of the cable carrying the UWTV signal to the surface. An additional and significant delay to the start of operations was lost time involved in trying to 'un-twist' the UWTV umbilical cable. The effects of weather and UWTV cable replacement on the rate of drilling are demonstrated in Figure 2.

Figure 2. Chart demonstrating operations by day, from which it is apparent that "untwisting" the UWTV camera cable resulted in significantly more delays to drilling than weather.

Core retrieval through >7000 m of drill string

Despite use of a plastic liner, a significant portion of the core was washed out of the drill string during recovery to the surface. The final core recovery proportion (38.9%) is less than typically observed (74.3%) from D/V *Chikyu*.

Installation of a temperature observatory

Because of technical problems and time constraints, it was not possible to install the temperature observatory planned across the fault zone during the main expedition. However, an additional 2 weeks of ship time later because available in July 2012. With the experience gained from the main expedition about the drilling conditions and improved engineering procedures, a borehole was quickly drilled through the fault zone and the temperature observatory installed. The string of temperature sensors were set within a 4.5 inch pipe about 820 m in length, which was placed into the borehole with relatively few problems.

PARTICLE ANALYSIS METHODS

Particle size was determined by sieving as follows: Wet sieving through 4ϕ sieve removed fines. Remaining material was dry sieved through -4ϕ to 3ϕ in 0.5ϕ intervals by mechanical shaking for 8 mins/sample. Weights retained on each sieve were converted to equivalent number of spherical grains by

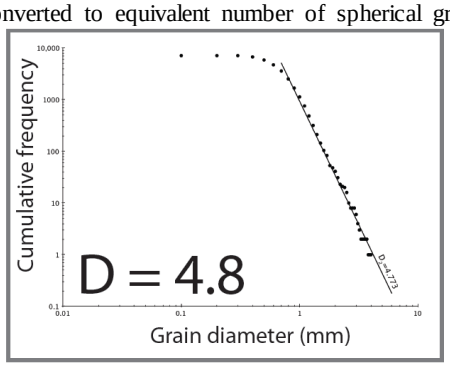

Figure 3. Example of determination of fractal dimension (D) of a particle size distribution

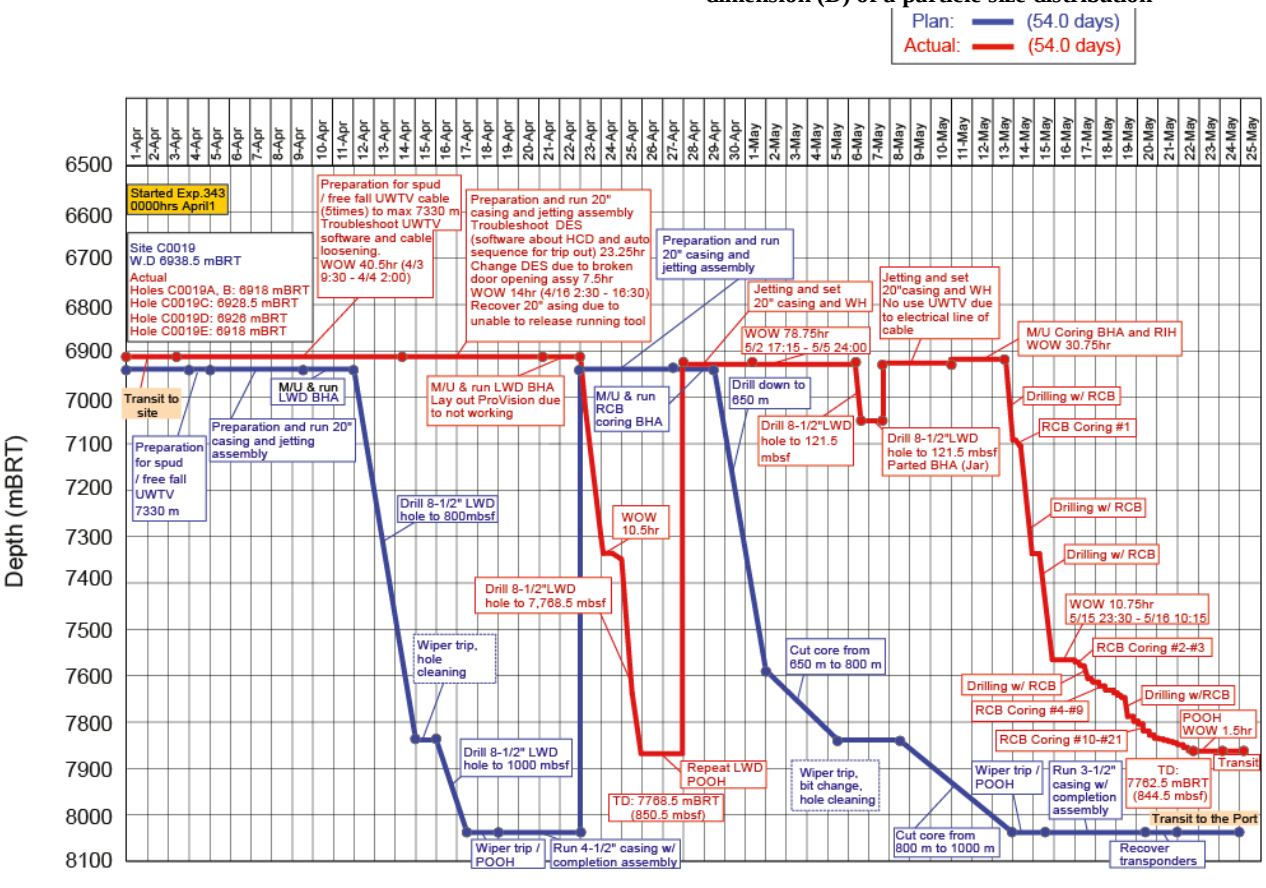

assuming all weight of material trapped was composed of grains with the maximum dimension of the sieve.

Cumulative frequency graphs were plotted to determine fractal dimensions (D; the inverse slope of the log cumulative frequency plots) of particle size distributions, PSD (Figure 3).

Particle size and shape were measured from flatbed scans of particles processed using the *Greyscale Image Analysis* Matlab routine as described by Bjoerk et al. (2009). Particle parameters indicated in Table 1 were measured using ImageJ. These parameters were combined into particle shape descriptors as outlined in Table 2.

Basic Measurement	Symbol	Explanation
Area	A	Area of the shape
Perimeter	P	Perimeter of the shape (length)
Area of the convex envelop	AE	Area of the convex envelop of a shape
Perimeter of the convex envelop	PE	Perimeter of the convex envelope of a shape
Long Axis	L	Length of the longest projection of the best fit ellipse
Short Axis	S	Length of the shortest projection of the best fit ellipse
Equivalent radius	r_{equ}	$r_{equ} = \sqrt{A/\pi}$
Equivalent diameter	d	$d=2 \cdot r_{equ}$
Feret diameter	$F_{max}h$	Maximum distance between parallel tangents touching the opposite sides of the particle also the width of the bounding rectangle
90 degrees to Feret diameter	$F_{max90}w$	Maximum distance between parallel also the height of the bounding rectangle

Table 1. Measured particle parameters

Shape descriptor	Equation
Sphericity	$\frac{2.\sqrt{\pi.A}}{P}$
Roundness (feret)	$\frac{4.A}{\pi.F^2}$
Rectangularity	$\frac{A}{w.h}$
Compactness	$\frac{d_{equ}}{P}$
Solidity	$\frac{A}{AE}$
Round	$\frac{4.A}{\pi.L^2}$
Circularity	$\frac{4.\pi.A}{P^2}$

Table 2. Particle shape descriptor definitions

PARTICLE ANALYSIS RESULTS

Particle size:
In combined sieve data all PSD are best fit by more than one D value. In the in situ (cores 2R and 3R) samples, smaller particles <~1 mm diameter, have D~1-1.5. In these samples, particles from 1-10 mm diameter have D > 4. In the transported sample (between cores 6R and 7R, the very small particles (<1 mm) and the coarse particles (>1 mm) also have fairly high D. Intermediate sized particles have similar D to finer particles in in situ samples.

Image analysis yields PSD with very low D and non-linear curves for clasts <~1 mm. Larger clasts (>~1 mm) have remarkably consistent D between samples, namely brown clasts have D~4.3 and grey clasts have D~4.5. Mean particle sizes (Figure 4) are smaller in grey than brown clasts within each sample. However, there is no systematic trend of mean particle size when all samples are considered.

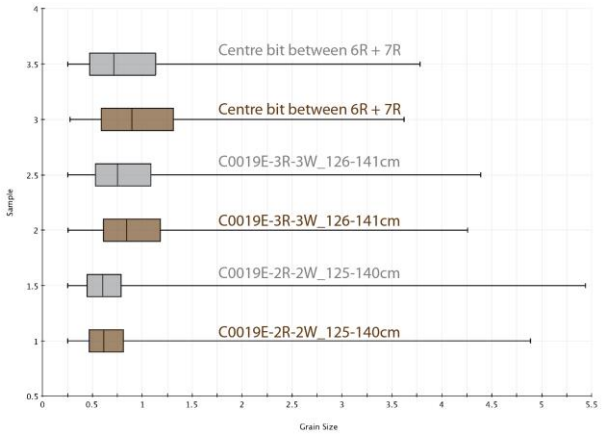

Figure 4. Box and whisker plots demonstrating grain sizes determined by image analysis.

Particle shape: There is no statistical difference in many of the shape descriptors for the grey and brown clasts. Grey clasts, particularly those in the 2ϕ range, display slightly higher mean roundness (particularly if measured using the major axis length) and circularity. The range of almost all parameters is greater for grey than brown clasts, particularly the grey transported clasts. The range is also generally larger in the smaller size fractions. In combined shape descriptor plots (e.g. Figure 5, typical of all samples), N(grey) is greater in all samples, and the grey clasts are more widely distributed across the graph in all samples.

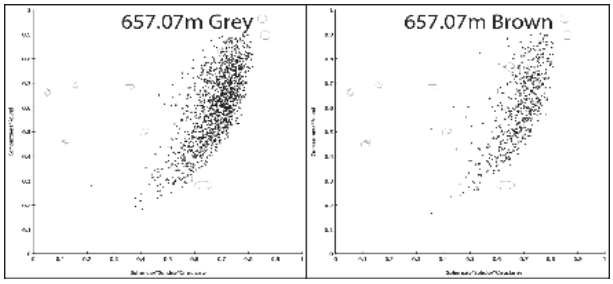

Figure 5. Sphericity x solidity x circularity vs. compactness x roundness. The distribution and relationship between different colour clasts is typical of all analysed samples.

DISCUSSION

General distribution of particle sizes and relation to mechanical processes during comminution
The high fractal dimension of the fine fraction in the transported sample reflects easy transport of finer material down the core barrel so these sizes are over-represented. A lack of difference in D of grey and brown clasts, suggests little difference in mechanical behaviour during fragmentation. Smaller mean grain size in grey clasts suggests they are overall slightly softer.

Theoretically 'constrained comminution' yields a PSD with D = 2.58 (Sammis et al., 1987). Blenkinsop (1991) determined PSD ranging from 1.88-3.08 in naturally fragmented rock, higher where alteration also played a role. D increase with strain. D of the fine fraction of drilling-induced breccias are less than these values, reflecting either that these breccias are 'unevolved' and D would increase with further wear, that constrained comminution did not occur, or undersampling? D in the coarse fraction are greated than expected if particle size

reduction occurred by constrained comminution implying the coarsest particles were 'selectively fragmented', or coarse fraction under-sampled?

Ability to resolve differences in shape using automated methods

The observation that grey clasts are rounder is only just detected by quantitative image analysis methods. Differences in roundness are better characterised based on the major axis length, which reflects that these particles are more elongate/tabular. It is not yet clear why there is a difference in mean shape descriptors and their range in different size fractions, nor why the grey clasts show more variation in shape overall.

Relationship between drilling and particle parameters

The variation in rate of mechanical work expended in drilling can be estimated from variation in drilling parameters such as rate of penetration (ROP), weight on bit (WOB) and rate of rotation (expressed as revolutions per minute; RPM). These parameters are illustrated in Figure 6. Also marked are depths from which the gravel samples were collected. It is apparent that there is no systematic difference in any of the drilling parameters between the various sample depths so this cannot explain differences in measured particle parameters. However, WOB was lower than average during drilling through these intervals, suggesting less mechanical work had to be expended to break the rock, thus that it was inherently weak and liable to easily degenerate during core retrieval.

CONCLUSIONS

It is possible to drill in >7000 m water depth but technical challenges such as borehole re-entry and core retrieval issues will be encountered. However, if these challenges can be overcome, excellent scientific results are possible.

Automated measurements of particle size and shape offer potential to understand fragmentation mechanics but methodologies require further development.

Figure 6. Variation in drilling parameters with depth in borehole C0019B. Red horizontal lines show depths of samples shown in Figures 4 and 5.

There is no systematic relationship between drilling parameters and size or shape of particles found in the core barrel, suggesting the latter result from damage to the core during retrieval, not directly from fragmentation during drilling. It was fairly easy to drill the gravel-producing layers, suggesting they were particularly weak and thus would have easily degenerated as the core was washed during retrieval within the plastic liner.

ACKNOWLEDGMENTS

We gratefully acknowledge financial and logistical support from IODP and the Australian-New Zealand IODP Consortium (ANZIC) for this research.

REFERENCES

Bjoerk, T., Mair, K., and Austrheim, H. 2009. Quantifying granular material and deformation: Advantages of combining grain size, shape, and mineral phase recognition analysis. Journal of Structural Geology 31(7), 637-653.

Blenkinsop, T. 1991. Cataclasis and mechanisms of particle size reduction. Paleogeophysics 136s(1), 59.

Chester, J., Chester F., and Kronenberg, A. 2005. Fracture surface energy of the Punchbowl fault, San Andreas system. Nature 437, 133-136.

Chester, F.M., Mori, J.J., Toczko, S., Eguchi, N., and the Expedition 343/343T Scientists, 2012. Japan Trench Fast Drilling Project (JFAST). IODP Prel. Rept., 343/343T. doi:10.2204/iodp.pr.343343T.

Sammis, C., King, G., and Biegel, R. 1987. The kinematics of gouge deformation. Pure and Applied Geophysics 125(5), 777-812

Stünitz, H., Keulen, N., Hirose, T., and Heilbronner, R 2010. Grain size distributions and microstructures of experimentally sheared granitoid gouge at coseismic slip rates – criteria to distinguish seismic and aseismic faults? Journal of Structural Geology 32, 59-69.